空间整形飞秒激光加工金属微细槽实验研究

梁密生，李欣*，王猛猛，原永玖，陈孝喆，许晨阳，左佩

北京理工大学机械与车辆学院激光微纳制造实验室，北京　100081

摘要　金属微细槽在电子、通信、航空航天、生物医学等领域有着广泛的应用。超快激光加工在 100 μm 及以下尺寸的微细槽加工中具有较大的潜力。为了提高金属微细槽的加工精度和加工质量，减小槽壁斜度，采用空间整形飞秒激光加工的方法，应用空间光调制器将高斯光整形为矩形平顶光，在高温合金上进行微细槽加工实验。结果表明，空间整形飞秒激光加工微细槽的槽壁斜度相较于高斯光束的加工结果明显减小，加工质量明显提高。此外，采用该方法分别加工了宽度为 10，20，150 μm 的深槽，结果显示，深槽槽壁截面未出现明显的热影响区域，说明该方法具有卓越的加工能力和极大的应用潜力。

关键词　激光技术；飞秒激光；空间整形；金属；微细槽

中图分类号　O436　　　　**文献标志码**　A　　　　　　　　　　**doi**：10.3788/CJL202148.0202003

1　引　　言

作为一种典型的金属微细结构，金属微细槽结构已被广泛地应用于电子、通信、航空航天、生物医学等领域。随着金属微细槽结构在关键零件上的应用越来越多，对微细槽的质量以及精度等提出了越来越高的要求[1-3]。在微型热交换装置中，具有矩形截面微细槽阵列结构的散热管相比其他形状的微细槽阵列结构具有更好的热传递性能，并且宽度小于 50 μm 的微细槽具有更高的热交换效率[4-5]。此外，在生物医学领域，小于 50 μm 的矩形微细槽阵列被证明比 60 μm 的矩形微细槽阵列具有更好的细胞定向效果[6-8]。微细槽结构精密制造往往需要较高的加工精度（100 μm 以内），加工边缘无毛刺，且常在许多高硬度、高韧性、高耐磨性的难加工材料上进行加工[9-10]。传统的金属加工方法比如传统切削、电火花加工、电解加工等在加工高精度金属微结构时，常会遇到精度不高或者材料加工难度大等问题，这使得微细槽结构精密制造一直是学术研究的热点[11-17]。国内外研究人员提出了多种加工方法来提高微细槽结构的加工精度和加工质量。南京航空航天大学的齐新新[18]在 100 μm 厚的不锈钢箔片上实现了平均缝宽为 166.65 μm、深度为 24.34 μm 的 5 条微细槽稳定加工。中国工程物理研究所的尹青峰等[19]通过工艺实验，优选工艺参数，成功地在 0.2 mm 厚的不锈钢薄片上加工出 0.15 mm 深的微细槽。山东大学的魏志远[20]采用超声振动辅助电解电火花铣削加工工艺，实现了 119.2 μm 宽度的微细槽加工。然而，目前大多数工艺加工的微细槽结构都在百微米量级，对于 100 μm 以内的微细槽结构高质量成型，尤其是 50 μm 以内的微细槽结构精密加工，仍然是当前研究的难点和热点。

超快激光加工具有瞬时功率密度高、热影响区小、可加工材料广泛等优点，在精密加工中发挥着越来越重要的作用[21-24]。尤其是对陶瓷材料、高温合金、超硬材料等难加工材料而言，超快激光加工已经成为一种必不可少的加工手段[25]。目前，超快激光在微小孔精密加工领域的优势已经逐渐得到认可[26]。德国米特韦达大学激光技术学院使用脉宽为 220 fs，频率为 100 kHz 的飞秒激光器在 304 不锈钢上加工出直径约 10 μm，深度达 500 μm 的微孔，微孔锥度为 10°[27]。通用原子公司在国家点火装置的钽准直仪中用飞秒激光

钻孔,各个孔的直径约为 200 μm[28]。在微细槽结构的加工方面,超快激光加工也逐渐走进人们的视野。日本芝浦工业大学表面工程设计实验室开发的飞秒激光加工系统,其光斑的最小直径为 1 μm,可加工出宽度为 5~10 μm 的金属微细槽[29]。Oh 等[30]利用激光刻蚀技术在不锈钢表面加工出深宽比为 4 的微米级微细槽结构。在微细槽的高精度加工方面,超快激光加工表现出巨大的优势。然而,由于加工过程中引起光斑分布不均以及屏蔽效应等[31],加工得到的微细槽槽壁往往会出现一定的斜度,从而影响其应用性能。因此,在保证精度的同时,如何减小槽壁的斜度是迫切需要解决的问题。

    基于光束整形原理,本文采用搭建的超快激光空间整形加工系统,将聚焦前的高斯光束调制成矩形平顶光,探索了光束空间整形对于微细槽结构形貌的影响以及锥度的减小情况。以镍基高温合金为例,相较于高斯光束的加工结果,采用矩形平顶光加工的微细槽槽壁斜度明显减小,且随着槽深的逐渐增大,槽壁斜度逐渐减小。此外,采用该方法在加工宽度分别为 10,20,150 μm 的深槽的过程中未出现明显的热影响区域,展示了该方法卓越的加工能力和极大应用潜力。

2 实验原理

2.1 实验装置及原理

    利用本课题组现有的飞秒激光加工实验系统进行实验探究,采用空间光调制器(SLM)对飞秒激光进行相位整形。本实验采用钛-蓝宝石激光器,出射的飞秒激光波长为 800 nm,脉宽为 50 fs,频率为 1 kHz。SLM 的型号为 holoeye-PLUTO-NIR-01,像素面积为 8 μm×8 μm,刷新率为 60 Hz。加工实验是在恒定温度(20 ℃)下进行的。样品固定于六轴平移台表面,通过计算机程序实现样品的运动控制,飞秒激光入射到 SLM 的液晶表面,经过相位整形后射出,再经过 4f 系统和物镜聚焦后对样品表面进行加工。图 1 为实验光路和装置原理图。需要说明的是,采用 SLM 进行相位调制后会有 40% 的功率损耗。本实验使用灰度图实现对像素电压的控制,在MALAB 软件中利用迭代算法计算目标光斑的初始相位,得到矩形平顶光斑,如图 2 所示。
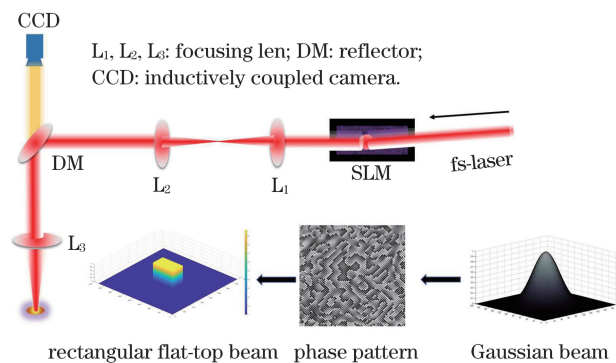

图 1 基于 SLM 的飞秒激光空间整形光路装置图

Fig. 1 Optical path device diagram of femtosecond laser spatial-shaping based on SLM
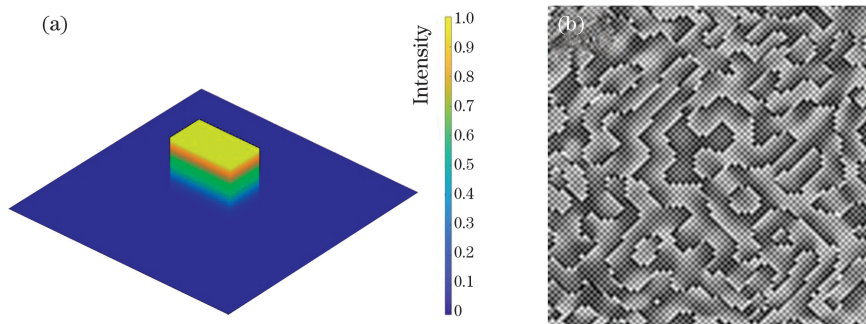
图 2 矩形平顶光的仿真示意图与灰度图。(a) 矩形光斑仿真示意图;(b)利用迭代算法得到的灰度图

Fig. 2 Simulation diagram of rectangular flat-top beam and grayscale image. (a) Simulation diagram of a rectangular spot; (b) grayscale image obtained by an iterative algorithm

2.2 矩形光斑的实际光强分布及显微镜下观测结果

    通过程序将灰度图加载至 SLM 后,采用光束质量分析仪对 SLM 整形后聚焦得到的矩形平顶光斑进行实时测量,测量结果如图 3(a)所示。某一点的亮度越高,表示光强越强。从图 3(a)可以看出,光斑的形状为明显的矩形,而且矩形的亮度比较均匀,边缘较为清晰。采用聚焦物镜对该光斑聚焦后,在高温合金表面进行脉冲打点实验,得到高温合金表面的实际加工形貌随着脉冲数增加的变化过程,如图 3(b)~(d)所示。
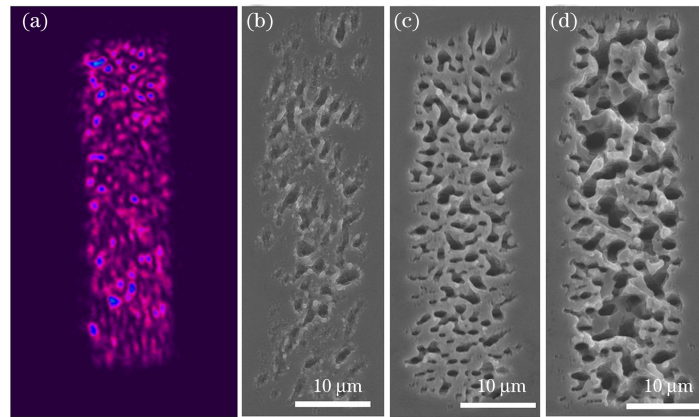
图 3　整形后的光斑表征及脉冲打点表征。(a)光束质量分析仪测得的矩形平顶光光斑分布；(b) 20 个脉冲下的高温合金表面加工形貌；(c) 100 个脉冲下的高温合金表面加工形貌；(d) 500 个脉冲下的高温合金表面加工形貌

Fig. 3　Characterization of light spot and pulse dot after shaping. (a) Light spot distribution of rectangular flat-top light measured by a beam quality profiler; (b) morphological image of surface with 20 pulses flat-top light ablation; (c) morphological image of surface with 100 pulses flat-top light ablation; (d) morphological image of surface with 500 pulses flat-top light ablation

3　实验结果与分析

为了对比高斯光与矩形平顶光的加工质量，采用焦点线扫的方式，以相同的扫描速度(500 μm/s)和扫描次数在高温合金表面进行微细槽加工实验。合金为镍基高温合金，牌号为 gh2135。白光干涉仪的型号为 ZYGONexView。采用高斯光进行微细槽加工时，用 10 × 物镜进行聚焦，脉冲能量为 20 μJ，以 500 μm/s 的扫描速度进行线扫加工。通过增加扫描次数的方式来增加微细槽深度，得到的微细槽阵列如图 4(a)所示。同样，采用整形后的光斑在高温合金表面进行聚焦加工，用 20 × 物镜进行聚焦，脉冲能量为 100 μJ，以 500 μm/s 的扫描速度进行线扫加工，通过增加扫描次数来增加微细槽的深度，得到的细槽阵列形貌如图 4(b)所示。从图 4(a)和图 4(b)可以看出，随着扫描次数的增加，整形光
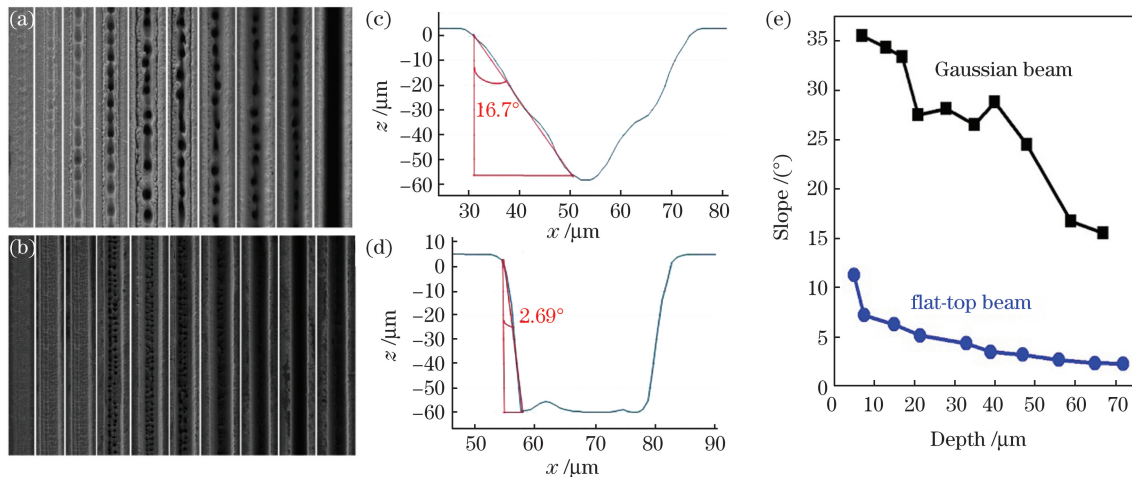
图 4　采用高斯光和平顶光加工的微细槽阵列对比。(a)采用高斯光加工的微细槽阵列形貌；(b) 采用平顶光加工的微细槽阵列形貌；(c) 采用高斯光扫描 100 次加工的单个微细槽截面轮廓；(d)采用平顶光扫描 100 次加工的单个微细槽截面轮廓；(e)微细槽阵列的深度与斜度的变化关系

Fig. 4　Comparison of microgroove array processed by Gaussian beam and flat-top beam. (a) SEM image of microgroove array fabricated by Gaussian beam; (b) SEM image of microgroove array fabricated by flat-top beam; (c) cross-sectional profile of a single microgroove (100 scanning times) fabricated by Gaussian beam; (d) cross-sectional profile of a single microgroove (100 scanning times) fabricated by flat-top beam; (e) relationship between the depth and the slope of the microgroove arrays

斑加工的微细槽底部的质量明显优于高斯光斑的加工质量。图 4(c)和图 4(d)分别展示了高斯光斑和矩形平顶光斑加工的微细槽截面轮廓,其中 x、y、z 表示相应的坐标轴。可以明显地看到,相较于高斯光加工的微细槽,矩形平顶光加工的微细槽截面轮廓更接近于矩形,且槽壁斜度明显减小。分析认为,这主要是由两种聚焦光斑的光斑能量分布不同引起的。高斯光斑的能量分布服从高斯分布,中心区域光强大,去除效率高,边缘区域光强相较于中心区域显著减小,导致材料去除效率较低,从而使得微细槽成型过程中材料去除不均匀,形成了较大的斜度。整形后的矩形平顶光斑能量分布较为均匀,材料去除均匀,因此槽壁斜度较小,且槽底较为平坦。图 4(e)所示为两种光斑加工的微细槽阵列斜度随深度的变化关系。可以看出,在两种加工方式下,微细槽壁斜度随着微细槽深度增加逐渐变小。在相近的深度下,采用矩形平顶光加工的微细槽斜度相较于高斯光加工的微细槽斜度显著减小。

在一定的激光脉冲频率下,扫描速度会影响沉积的脉冲数量,进而影响材料的去除速率。为了分析扫描速度对矩形平顶光加工微细槽的影响,在相同的脉冲能量(100 μJ)下,分别采用 2000,1000,500 μm/s 的扫描速度,在高温合金表面进行微细槽阵列加工。在特定的扫描速度下,通过增加扫描次数来改变微细槽的深度,进而得到不同扫描速度下深度不同的微细槽阵列。对上述 3 个扫描速度下的微细槽阵列三维形貌和微细槽截面轮廓进行对比,结果如图 5 所示。在 2000 μm/s 的扫描速度下,随着扫描次数的增加,微细槽的深度逐渐增加,且深度变化率先增大后减小。在 1000 μm/s 和 500 μm/s 的扫描速度下,微细槽的深度随着扫描次数的增加逐渐增大,且深度变化率未明显减小。分析认为,随着扫描速度的增大,高温合金单位面积内沉积的脉冲数量减少,在达到一定深度后,槽底的加工碎屑增多,屏蔽效应增强,导致单个脉冲的材料去除量减小。从截面轮廓来看,3 个扫描速度下的微细槽阵列都呈现出上宽下窄的特征,且槽顶部和底部的宽度差值较为稳定,受扫描速度的影响较小。
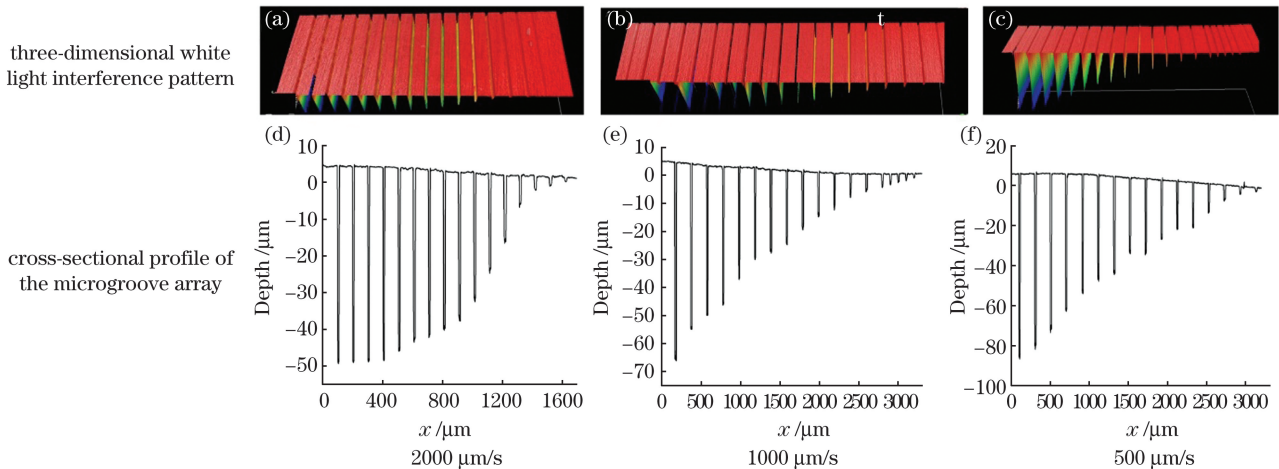
图 5 矩形平顶光在不同扫描速度下加工的微细槽对比

Fig. 5 Comparison of microgrooves fabricated by flat-top beam at different scanning speeds

此外,研究了不同激光能量下以及不同扫描速度下的微细槽深度和微细槽壁斜度的变化规律。从图 6(a)可以看出,在相同能量下,随着扫描次数的增多,微细槽的深度逐渐增加,因此可以结合激光脉冲能量和扫描次数实现微细槽加工深度的控制。然而,在各个能量下,扫描深度的增长量随着扫描次数增加逐渐变小,这是因为随着深度增加,加工点逐渐偏离焦平面,导致加工能力下降。另外,随着加工深度逐渐变大,加工碎屑无法即时排出,导致加工效率变低。因此,可以随着加工深度变化逐渐加深焦点位置,或者增加吹气设备及时去除加工碎屑。图 6(b)展示了不同能量下槽壁斜度随微细槽深度的变化情况。可以看出,随着微细槽深度增加,槽壁斜度逐渐减小,槽壁斜度最小值可以达到 1°以下。当微细槽深度相同时,槽壁斜度相近,并没有因为能量的不同出现明显的差异,这主要是因为在微细槽成型过程中激光能量主要影响材料去除速率,而槽壁的形状主要取决于加工光斑的能量分布。

图 6 不同脉冲能量下微细槽深度和微细槽壁斜度的变化情况。(a)微细槽深度随扫描次数的变化情况；(b) 微细槽壁斜度随深度和扫描次数的变化情况

Fig. 6 Variation of depth and slope of microgrooves under different pulse energies. (a) Depth of microgrooves changed with scanning times; (b) slope of microgrooves changed with microgroove depth and scanning times
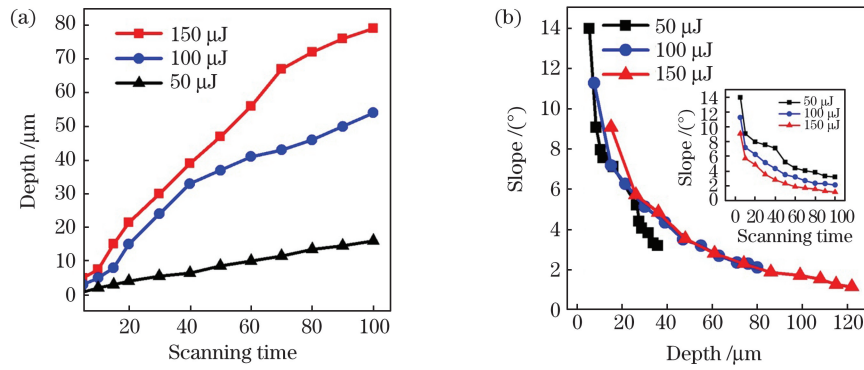
为了证明空间整形的矩形平顶光束在微细槽加工领域的应用潜力，采用逐行扫描加工的方式进行变宽度微细槽阵列加工实验。在 100 μJ 的脉冲能量下，控制扫描速度为 1000 μm/s，扫描次数为 40 次，扫描间距为 5 μm。通过逐渐增大扫描宽度的方式来控制微细槽的深度，实现了槽宽从 10 μm 到 60 μm 的变宽度微细槽加工，得到的微细槽阵列的表面形貌如图 7(a)所示。从形貌图可以看到，微细槽的宽度逐渐增大，且边缘平直整齐。图 7(b)为微细槽阵列的横截面轮廓图。可以看到，微细槽的侧壁斜度未随着深度的增加有明显的变化。可以推断，侧壁斜度的关键影响因素是形成侧壁时的焦点光斑能量分布。这主要是因为飞秒激光具有优异的冷加工能力，在与金属材料作用时，在极短的时间内与材料发生作用并将材料去除，将热影响限制在焦点与材料作用的区域，减小了对加工光斑以外区域的影响。

激光加工已经作为一项比较成熟的技术广泛地应用于微细槽结构的加工中（表 1）。然而，不同于一般的长脉冲激光或者连续激光利用热效应去除材料的机理，飞秒激光与高温合金材料的能量传递过
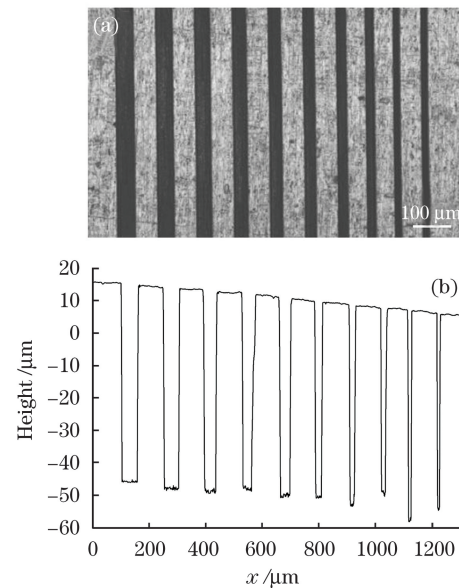
图 7 采用空间整形光束加工的变宽度微细槽阵列。(a)变宽度微细槽阵列的表面形貌图；(b)微细槽阵列截面轮廓图

Fig. 7 Microgroove arrays with variable width processed by spatially shaped beam. (a) Surface morphology of the microgroove array; (b) cross-sectional profile of microgroove array

表 1 现有激光加工微细槽情况小结

Table 1 Summary of existing laser microgroove processing

Laser-type	Material	Groove width /μm	Groove depth /μm	Slope /(°)
Nanosecond laser[32]	Ti_6Al_4V	14	10	23
Pulsed Nd：YAG laser[33]	Al_2O_3	13	12	＞20
Laser-induced thermochemical wet etching[34]	Stainless steel	15—50	300	11.5
Pulsed CO_2 laser[35]	ZrO_2	30—50	15—50	16
Pulsed Nd：YAG laser[36]	Aluminum	30	20	22
Nanosecond pulsed laser[37]	Sapphire	0—320	0—800	11.3

程可以由激光与金属作用的"改进双温方程"[38]进行描述。飞秒激光的脉宽极短(<100 fs),与材料作用的持续时间远小于电子-晶格能量弛豫时间($10^{-10} \sim 10^{-12}$ s),因此,激光脉冲能量被电子吸收的过程在高温合金晶格能量变化之前完成。在飞秒脉冲持续时间内,通过晶格进行的流体运动和热传导可以忽略不计。当光斑的空间分布被改变后,受热电子的分布区域也随之改变。在矩形平顶光斑辐照的区域内,电子温度在激光脉冲作用下急剧升高,然后电子-晶格系统开始进行能量耦合,被照射区域的材料以原子蒸气的方式离开基体。由于晶格的热传导在极短的时间内可以忽略不计,而受辐照区域材料被去除时带走了大部分的热量,极大地抑制了辐照区域外的能量传递。因此在微细槽成型过程中,矩形平顶光斑辐照的区域和附近其他区域也形成了强烈的对比:一方面平顶光斑辐照区域高温合金材料的电子温度瞬间升高,材料以原子蒸气等方式在短时间内被去除;另一方面,在未被矩形平顶光照射的区域,材料基本未接收到来自其他部位的能量,材料的电子和晶格状态未受到任何影响。因此,光斑能量分布是在高温合金微细槽成型过程中影响微细槽轮廓形状的关键因素。

图 8 所示为在高温合金样品上加工的深槽和通槽。除了槽宽较小的微细槽之外,还加工了槽宽为 150 μm 的深槽,如图 9 所示,证明了所提方法可以实现从 10 μm 到 100 μm 加工尺度的跨度。从图 9 可以看到,150 μm 宽槽的槽壁斜度约为 $0.63°$,此时该细槽接近于直槽。此外,还可以发现,宽槽的入口处有一个缓坡,这可能是反复扫描过程中激光光斑的额外能量影响的结果。

为了探究激光烧蚀过程对槽壁的影响,对图 9 所示的微细槽侧壁横截面进行元素分布检测,结果如图 10 所示。图 10(a)为微细槽侧壁横截面的高倍 SEM 形貌图,从形貌来看,微细槽侧壁未出现明显的热影响区域。图 10(b)~(e)所示分别为微细槽侧壁截面元素信号强度分布及 O 元素、Ni 元素和 Fe 元素在横向面上的分布情况。根据槽壁的截面形貌以及元素信号强度变化情况,可以判断出微细槽侧壁无明显氧化。这应当归功于飞秒激光卓越的冷加工能力:1)在加工过程中,飞秒激光的脉宽极短(50 fs),在这么短的时间内热量还未传递到加工区域外围,材料就已经被去除了,导致加工区域外围温度未升高,未产生明显氧化;2)飞秒激光加工过程中产生的瞬时等离子体对氧气具有隔绝效应。
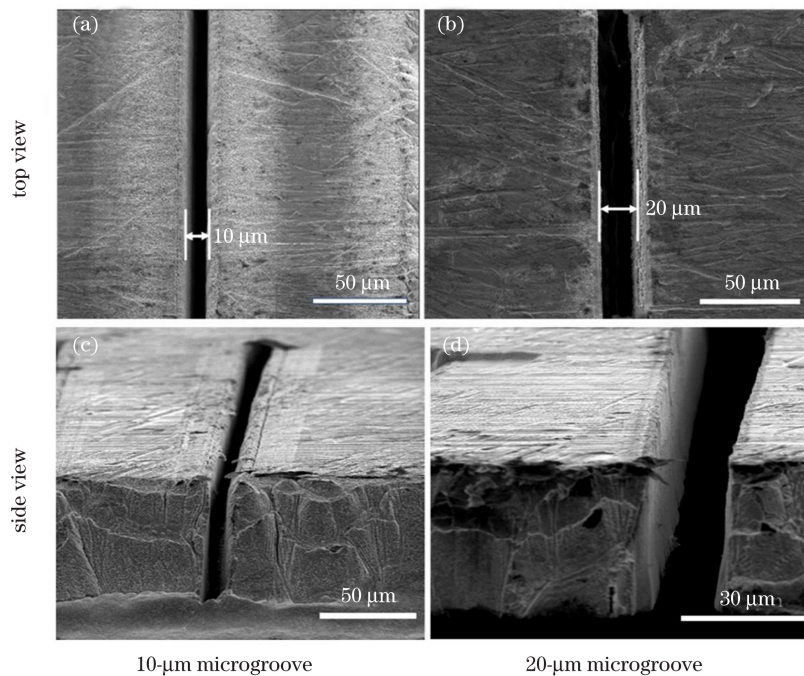
图 8 加工宽度为 10 μm 和 20 μm 的微细槽形貌图

Fig. 8 Topographies of microgrooves with width of 10 μm and 20 μm
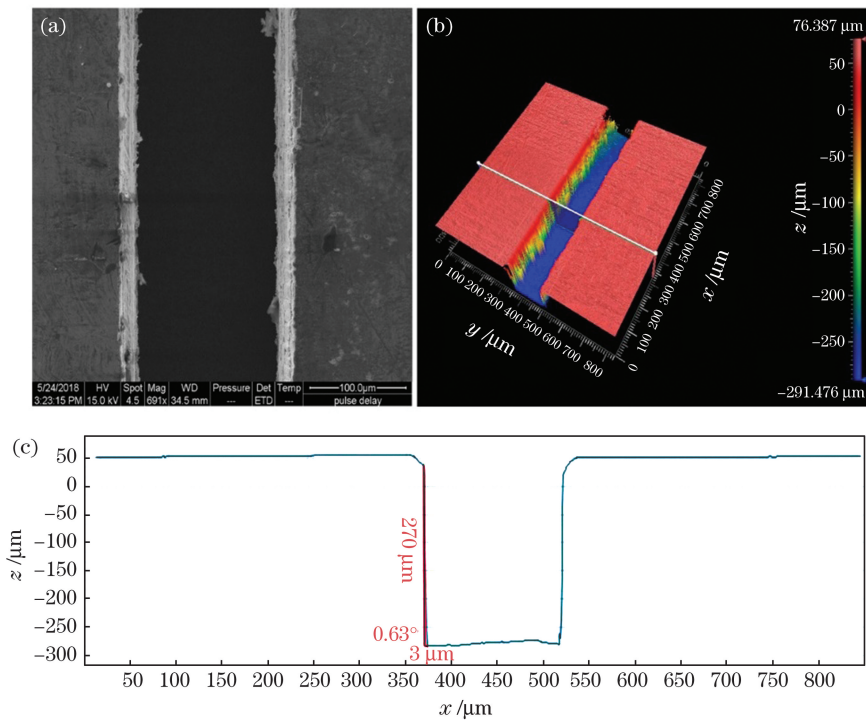
图 9　宽度为 150 μm 的微细槽形貌图。(a) SEM 图；(b)白光干涉三维图；(c)横截面轮廓图

Fig. 9　Topography of microgroove with width of 150 μm. (a) SEM image; (b) three-dimensional white light interference image; (c) cross-sectional profile view
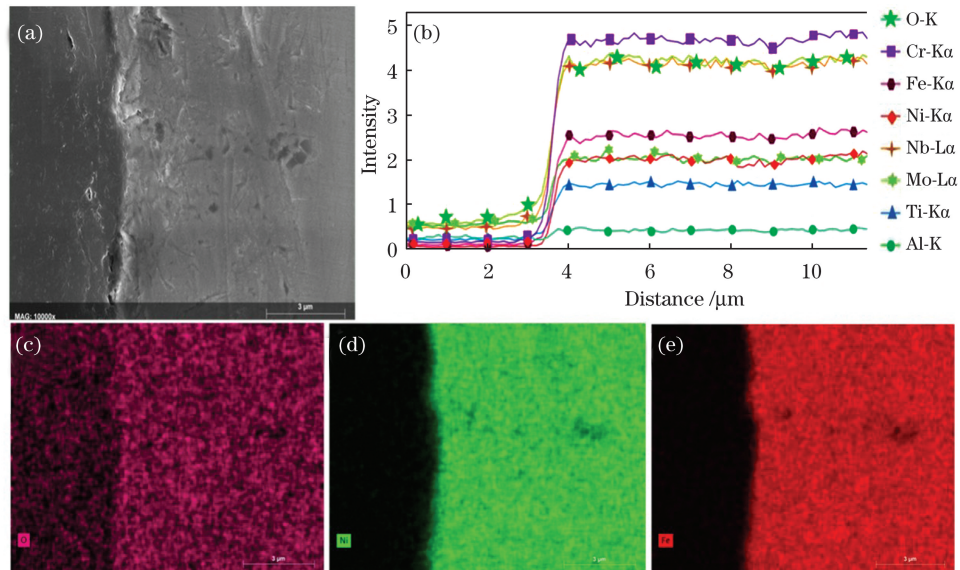
图 10　微细槽侧壁边缘元素分布及信号强度变化。(a)微细槽侧壁截面的 SEM 形貌图；(b)元素信号强度的横向分布；(c) O 元素在横向面的分布；(d) Ni 元素在横向面的分布；(e) Fe 元素在横向面的分布

Fig. 10　Distribution and intensity changes of elements at the processing edge of microgroove. (a) SEM image of the microgroove side wall section; (b) transverse distribution of element intensity; (c) distribution of O element in the transverse plane; (d) distribution of Ni element in the transverse plane; (e) distribution of Fe element in the transverse plane

4　结　　论

本研究采用空间整形飞秒激光加工的方法，利用 SLM 将高斯光束整形成矩形平顶光束后进行金属微细槽加工，相较于高斯光束的加工结果，利用矩形平顶光斑加工的槽壁斜度显著减小。采用该方法

实现了 10 μm 量级到 100 μm 量级的微细深槽加工,表明该方法具有较宽的加工尺度范围。对深槽槽壁截面进行元素分析和形貌观察,未发现元素含量明显变化的区域和明显的激光热影响区,说明该方法具有卓越的加工能力和极大的应用潜力。

参 考 文 献

[1] Wang Y F, Zhang T R, Zhang W W, et al. Study on laser processing technology of surface micro grooves for complex surface parts[J]. Electromachining & Mould, 2018(S1): 43-46.
王云峰, 张天润, 张文武, 等. 复杂曲面零件表层微槽激光加工技术研究[J]. 电加工与模具, 2018(S1): 43-46.

[2] Wang J J, Guo Z N, He J F, et al. Research on micro-ultrasonic-assisted high-speed microgroove milling process[J]. Modular Machine Tool & Automatic Manufacturing Technique, 2020(5): 119-123.
王俊杰, 郭钟宁, 何俊峰, 等. 微细超声辅助高速微槽铣削加工工艺研究[J]. 组合机床与自动化加工技术, 2020(5): 119-123.

[3] Shi Y, Xu B, Wu D, et al. Research progress on fabrication of functional microfluidic chips using femtosecond laser direct writing technology[J]. Chinese Journal of Lasers, 2019, 46(10): 1000001.
史杨, 许兵, 吴东, 等. 飞秒激光直写技术制备功能化微流控芯片研究进展[J]. 中国激光, 2019, 46(10): 1000001.

[4] Ternet F, Louahlia-Gualous H, Le Masson S. Impact of microgroove shape on flat miniature heat pipe efficiency[J]. Entropy, 2018, 20(1): 44.

[5] Ghajar M, Darabi J. Evaporative heat transfer analysis of a micro loop heat pipe with rectangular grooves[J]. International Journal of Thermal Sciences, 2014, 79: 51-59.

[6] Brunette D M. Fibroblasts on micromachined substrata orient hierarchically to grooves of different dimensions[J]. Experimental Cell Research, 1986, 164(1): 11-26.

[7] Fu G, Soboyejo W O. Cell/surface interactions of human osteo-sarcoma (HOS) cells and micro-patterned polydimelthylsiloxane (PDMS) surfaces[J]. Materials Science and Engineering C, 2009, 29(6): 2011-2018.

[8] Ren L, Zhou X W, Nasiri R, et al. Combined effects of electric stimulation and microgrooves in cardiac tissue-on-a-chip for drug screening[J]. Small Methods, 2020, 4(10): 2000438.

[9] Li W G, Zhou H W, Li K T. The process of micro groove machined by single point diamond machine tool[J]. Mechanical & Electrical Engineering Technology, 2018, 47(10): 7-10,86.
李伟国, 周欢伟, 李克天. 在单点金刚石机床上用刨削加工微槽的方法[J]. 机电工程技术, 2018, 47(10): 7-10,86.

[10] Li Y C, Zhang X B, Mao Z, et al. Study on size and morphology control of 316L stainless steel microgrooves processed by ultraviolet nanosecond laser[J]. Applied Laser, 2019, 39(6): 994-1001.
李元成, 张晓兵, 毛忠, 等. 紫外纳秒激光加工 316L 不锈钢微槽尺寸和形貌控制研究[J]. 应用激光, 2019, 39(6): 994-1001.

[11] Kuo C L, Huang J D. Fabrication of series-pattern micro-disk electrode and its application in machining micro-slit of less than 10 μm [J]. International Journal of Machine Tools and Manufacture, 2004, 44(5): 545-553.

[12] Lauwers B, Oosterling H, Vanderauwera W. Development of an operations evaluation system for sinking EDM[J]. CIRP Annals, 2010, 59(1): 223-226.

[13] Kirchner V, Cagnon L, Schuster R, et al. Electrochemical machining of stainless steel microelements with ultrashort voltage pulses [J]. Applied Physics Letters, 2001, 79(11): 1721-1723.

[14] Ya C. Internal laser writing of high-aspect-ratio microfluidic structures in silicate glasses for lab-on-a-chip applications[J]. Micromachines, 2017, 8(2): 59.

[15] Wang W, Zhu D, Qu N S, et al. Electrochemical drilling with vacuum extraction of electrolyte[J]. Journal of Materials Processing Technology, 2010, 210(2): 238-244.

[16] Li P T, Fu B, Jing Q, et al. Experimental research on milling micro-groove by wire-proposed electrochemical jet machining[J]. New Technology & New Process, 2020(4): 67-74.
李飘庭, 傅波, 荆奇, 等. 电极丝前置式射流电解加工铣削微槽试验研究[J]. 新技术新工艺, 2020(4): 67-74.

[17] Li Z Q, Zhao P J, Song Y X, et al. Research status of micro abrasive water jet machining technology[J]. Nanotechnology and Precision Engineering, 2016, 14(2): 134-144.
李增强, 赵佩杰, 宋雨轩, 等. 微磨料水射流加工技术研究现状[J]. 纳米技术与精密工程, 2016, 14(2): 134-144.

[18] Qi X X. Research on electrochemical machining of microgrooves in flexible metal sheet[D]. Nanjing: Nanjing University of Aeronautics and Astronautics, 2018.
齐新新. 柔性金属箔群槽微细电解加工技术研究[D]. 南京: 南京航空航天大学, 2018.

[19] Yin Q F, Li S N, Sheng Y P, et al. Micro milling of sheet parts [J]. Manufacturing Technology & Machine Tool, 2015(9): 115-117.
尹青峰, 李盛年, 盛友萍, 等. 薄片工件的微细铣削加工[J]. 制造技术与机床, 2015(9): 115-117.

[20] Wei Z Y. Study on ultrasonic vibration assisted micro electrochemical discharge machining technology[D]. Jinan: Shandong University, 2019.
魏志远. 超声振动辅助微细电解电火花加工技术研究[D]. 济南: 山东大学, 2019.

[21] Zhao L L. Experimental studies on fabrication of high-aspect-ratio microgrooves by femtosecond laser based on electron dynamics control [D]. Beijing: Beijing Institute of Technology, 2015: 8-17.
赵亮亮. 基于电子状态调控的飞秒激光加工高深宽比结构的实验研究[D]. 北京: 北京理工大学, 2015: 8-17.

[22] Song Y X, Yin K, Dong X R. Morphology and hydrophobicity of ZnS surface fabricated by femtosecond pulse laser[J]. Applied Laser, 2017, 37 (3): 398-402.
宋雨欣, 银恺, 董欣然. 飞秒激光加工 ZnS 晶体沟槽形貌及其疏水性能研究[J]. 应用激光, 2017, 37 (3): 398-402.

[23] Jiang L, Wang A D, Li B, et al. Electrons dynamics control by shaping femtosecond laser pulses in micro/nanofabrication: modeling, method, measurement and application[J]. Light: Science & Applications, 2018, 7(2): 17134.

[24] Ma Z C, Zhang Y L, Han B, et al. Femtosecond-laser direct writing of metallic micro/nanostructures: from fabrication strategies to future applications[J]. Small Methods, 2018, 2(7): 1700413.

[25] Wei C, Ma Y P, Han Y, et al. Femtosecond laser processing of ultrahard materials [J]. Laser & Optoelectronics Progress, 2019, 56(19): 190003.
魏超, 马玉平, 韩源, 等. 飞秒激光加工超硬材料的研究进展[J]. 激光与光电子学进展, 2019, 56(19): 190003.

[26] Guo M C, Wang M D, Zhang S J, et al. Research on femtosecond laser microhole processing technology of FR-4 copper clad laminate[J]. Chinese Journal of Lasers, 2020, 47(12): 1202008.
郭敏超, 王明娣, 张胜江, 等. FR-4 覆铜板飞秒激光微孔加工工艺研究[J]. 中国激光, 2020, 47(12): 1202008.

[27] Gruner A, Schille J, Loeschner U. Experimental study on micro hole drilling using ultrashort pulse laser radiation[J]. Physics Procedia, 2016, 83: 157-166.

[28] Laser micro-machining [EB/OL]. [2020-08-20]. https://www.ga.com/manufacturing-and-fabrication/laser-micro-machining.

[29] Aizawa T, Inohara T. Pico- and femtosecond laser micromachining for surface texturing micromachining [M]. Tokyo: Intech Open, 2019:4-15.

[30] Oh K H, Park J B, Cho S I, et al. Investigation of sidewall roughness of the microgrooves manufactured with laser-induced etching technique [J]. Applied Surface Science, 2009, 255(24): 9835-9839.

[31] Kerse C, Kalaycıoğlu H, Elahi P, et al. Ablation-cooled material removal with ultrafast bursts of pulses[J]. Nature, 2016, 537(7618): 84-88.

[32] Fasasi A Y, Mwenifumbo S, Rahbar N, et al. Nano-second UV laser processed micro-grooves on Ti_6Al_4V for biomedical applications[J]. Materials Science and Engineering: C, 2009, 29(1): 5-13.

[33] Ketabi M, Deporter D. The effects of laser microgrooves on hard and soft tissue attachment to implant collar surfaces: a literature review and interpretation [J]. The International Journal of Periodontics & Restorative Dentistry, 2013, 33(6): e145-e152.

[34] Oh K H, Lee M K, Jeong S H. Laser micromachining of high-aspect-ratio metallic channels for the application to microthermal devices [J]. Korean Journal of Optics and Photonics, 2006, 17 (5): 437-446.

[35] Liu Y Y, Liu L L, Deng J X, et al. Fabrication of micro-scale textured grooves on green ZrO_2 ceramics by pulsed laser ablation[J]. Ceramics International, 2017, 43(8): 6519-6531.

[36] Kikuchi T, Sakairi M, Takahashi H, et al. Fabrication of micropores and grooves on aluminum by laser irradiation and electrochemical technique[J]. Journal of the Electrochemical Society, 2001, 148 (11): C740-C745.

[37] Takayama N, Asaka S, Yan J W. Nanosecond pulsed laser irradiation of sapphire for developing microstructures with deep V-shaped grooves [J]. Precision Engineering, 2018, 52: 440-450.

[38] Jiang L, Tsai H L. Improved two-temperature model and its application in ultrashort laser heating of metal films[J]. Journal of Heat Transfer, 2005, 127(10): 1167-1173.

Spatially-Shaped Femtosecond Laser Manufacturing of Microgrooves in Metals

Liang Misheng, Li Xin[*], Wang Mengmeng, Yuan Yongjiu, Chen Xiaozhe,
Xu Chenyang, Zuo Pei

*Laser Micro/Nano Fabrication Laboratory, School of Mechanical Engineering, Beijing Institute of Technology,
Beijing 100081, China*

Abstract

Objective　As a typical metal microstructure, the metal microgroove structure is widely used in electronics, communications, aerospace, biomedicine, and other fields. With more applications of metal microgrooves in key parts, higher requirements are put forward on the quality and accuracy of microgrooves. For example, in the micro-heat exchange device, the heat transfer pipe with a rectangular cross-section microgroove array structure has better heat transfer performance than other shapes of the microgroove array structure, and the microgrooves with a width less than 50 μm show better heat exchange efficiency. In addition, in the field of biomedicine, rectangular microgroove arrays smaller than 50 μm have been proven to have better cell orientation effects than rectangular microgroove arrays of 60 μm. The precision manufacturing of microgroove structure often requires high machining accuracy (below 100 μm), and the machining edge is free of burrs. Besides, the microgroove structure is often processed on many difficult-to-machine materials with high hardness, toughness, and wear resistance. Traditional metal processing methods, such as traditional cutting, electric discharge machining, and electrochemical machining, are often troubled by insufficient precision or difficult material processing when processing high-precision metal microstructures. Ultrafast laser processing has the advantages of high instantaneous power density, low heat-affected zone, and a wide range of materials that can be processed, and it is playing an increasingly important role in precision processing. Ultrafast laser processing has become an essential processing method, especially for difficult-to-process materials such as ceramic materials, superalloys, and superhard materials. However, due to the uneven light field distribution and shielding effect caused by the processing process, the processed micro groove wall is often accompanied by a certain slope, which affects its application performance. Therefore, reducing the groove wall slope while ensuring accuracy is an urgent problem to be solved. In the present study, we adopt an spatial shaping ultrafast laser processing system, based on the principle of beam shaping, built to modulate the Gaussian beam before focusing on a rectangular flat-top light and explore the influence of spatial shaping light on the microgroove structure and reduction of taper.

Methods　In this study, the laboratory's existing femtosecond laser processing experimental system was used to conduct experimental investigations on nickel-based superalloys. The spatial light modulator (SLM) was used to phase-shape the femtosecond laser, and the Gaussian light was shaped into a rectangular flat-top light and the processing experiment of the microgroove was on the nickel-based superalloy. Then, the surface morphology and three-dimensional morphology of the microgrooves processed by the spatial shaping light were analyzed by scanning electron microscope (SEM) and three-dimensional white light interferometer. In the next step, by adjusting the laser parameters, the processing parameters of the microgroove using the spatial shaping light was studied, and the microgroove and through groove with variable width were processed. In addition, the surface morphology and chemical composition of the microgroove were analyzed by SEM and energy dispersive X-ray spectroscopy (EDX). In addition, the effect of femtosecond laser processing on the oxidation of the microgroove was studied by EDX mapping.

Results and Discussion　Compared with the Gaussian light, the slope of the microgroove obtained by the spatially shaped light is significantly reduced, and the groove wall profile is straighter. By comparing the effects of different scanning speeds at the same energy, it is found that at a scanning speed of 2000 μm/s, as the scanning time increases, the depth of the microgroove gradually increases, and the depth change rate first increases and then decreases. At scanning speeds of 1000 μm/s and 500 μm/s, the depth of the microgroov gradually increases with the increasing scanning speed, and the depth change rate gradually increases. The analysis shows that with the increase in the scanning speed, the number of pulses deposited in the unit area of the superalloy decreases. After reaching a certain depth, as the processing debris at the bottom of the groove increases, the shielding effect increases, so that

the average removed amount of a single pulse is reduced (Fig. 5). As the depth of the microgroove increases, the slope of the groove wall gradually decreases and the minimum slope of the groove wall can reach 1° or less (Fig. 6). In addition, deep grooves with width of 10, 20, and 150 μm were processed using spatial shaping light, and the groove wall slope of the deep grooves with a width of 150 μm reached 0.63° (Fig. 8 and Fig. 9). The elemental analysis and characterization of the groove wall found that the microgroove wall did not undergo significant oxidation, which should be attributed to the excellent cold working ability of the femtosecond laser (Fig. 10).

Conclusions In this study, the strategy of spatially shaped femtosecond laser is adopted and the Gaussian beam is formed into a rectangular flat-top beam by the SLM for metal microgroove processing. Compared with the processing result of the Gaussian beam, the slope of the groove wall fabricated by flat-top beam is significantly reduced. In addition, the method has been used to realize the processing of micro-deep grooves ranging from 10 μm to 100 μm, indicating that the method has a wide range of processing dimensions. Elemental analysis and morphological observation of the deep groove wall section were carried out. No obvious element changes and laser heat-affected zone were found, indicating the excellent processing ability and great application potential of this method.

Key words laser technique; femtosecond laser; spatial shaping; metal; microgroove

OCIS codes 140.3538; 140.3390